Reaction Kinetics, Mechanisms and Catalysis (2024) 137:1031–1049
https://doi.org/10.1007/s11144-024-02586-1

# Kinetic and isothermal studies of naproxen adsorption from aqueous solutions using walnut shell biochar

**Rukiye Şensoy[1] · Burcu Kabak[1] · Erdal Kendüzler[1]**

Received: 1 November 2023 / Accepted: 30 January 2024 / Published online: 7 February 2024


## Abstract

In this study, biochar was obtained from walnut shells (WS) using one- and two-stage pyrolysis processes at different temperatures (500, 600, 700, 700 + 700 °C). The biochar obtained was used as an adsorbent for the removal of naproxen, an organic pollutant, from aquatic systems. The highest removal efficiency was obtained with 700 + 700-WSB obtained by the two-stage pyrolysis method. The physicochemical properties of walnut shell biochar (WSB) were investigated using SEM–EDX, FTIR, XRD, BET, elemental analysis, and TGA. 700 + 700-WSB had a high surface area of 649 $m^2$/g and a pronounced porous structure, according to the BET and SEM analysis results. Various experimental parameters (pH, contact time, amount of adsorbent, temperature, initial concentration, and $pH_{pzc}$) were investigated to study the adsorption of naproxen by 700 + 700-WSB in an aqueous solution. The point of zero charge of the 700 + 700-WSB adsorbent was calculated as 7.15. The 700 + 700-WSB obtained at optimum parameter levels, such as 25 °C and 4 h time has an adsorption capacity of 58.8 mg/g. To analyze the equilibrium results, the Langmuir, Sips, Freundlich, and Temkin adsorption isotherm models were utilized. The equilibrium data fit the Langmuir ($R^2 = 0.984$) and Sips ($R^2 = 0.979$) models among the isotherm models. Investigating the adsorption characteristics of naproxen on WSB involved the study of the kinetic models and thermodynamic components of the adsorption process. The psuedo-second order kinetic model (PSO) was shown to be consistent with the experimental data through kinetic investigations, and the thermodynamic results ($\Delta G° = -21.87$ kJ/mol, $\Delta H° = -29.52$ kJ/mol and $\Delta S° = -25.73$ J/mol K) indicated that the adsorption process was exothermic and spontaneous.

✉ Erdal Kendüzler
kenduzler@mehmetakif.edu.tr

[1] Faculty of Arts and Science, Chemistry Department, Burdur Mehmet Akif Ersoy University, 15100 Burdur, Turkey

## Graphical Abstract

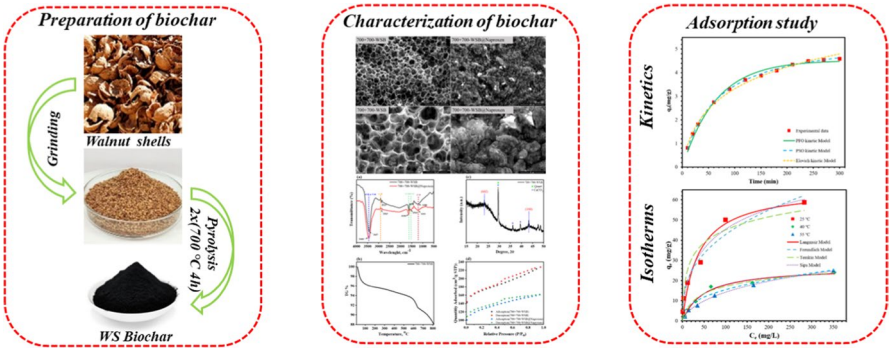


**Keywords** Adsorption · Biochar · Naproxen · Walnut shell · Wastewater treatment

## Introduction

Contamination of water bodies with pharmaceuticals has become a growing concern worldwide. Nonsteroidal anti-inflammatory drugs (NSAIDs) are a class of medications that are used extensively worldwide to treat pain and inflammation. [1]. Since this group of drugs is easily available without a prescription, it is one of the leading pharmaceutical compounds that pollutes the environment quickly and uncontrollably [2]. Naproxen, belonging to the NSAID class, is a pain reliever that is widely used in the treatment of many diseases, such as degenerative joint disease, rheumatoid arthritis, acute gout, pain, and inflammation [3, 4]. Consequently, it is consumed in significant amounts by both humans and animals. Approximately 72% of the naproxen excreted has the propensity to undergo hydrolysis and subsequently enter aquatic ecosystems [5, 6]. The World Health Organization (WHO) has verified the existence of high-dose drugs ranging from to 15–25 µg/L in drinking water [7, 8]. Long-term accumulation of pharmaceutical compounds, such as naproxen, in water and soil causes toxic effects, which are dangerous for living organisms [9]. Therefore, the removal of naproxen and other drug residues from water sources is important [10].

Many different methods are used for the removal of pharmaceutical compounds from aquatic environments. Examples of these methods include electrochemical oxidation [11], membranes [12], coagulation-ozonation [13], ultrasonic cavitation treatment [14], photocatalysis [15], bio-electrochemical oxidation [16], volatilization [17], sedimentation [18], Fenton-based processes [19], and adsorption [20–22]. Among these methods, the adsorption method is preferred because of its simpler design, high efficiency, low-cost operation, and excellent performance [23].

One of the most important aspects of the adsorption process is adsorbent selection. A wide variety of adsorbents have been used in adsorption studies, such as

zeolites [24], clay [25], carbon nanotubes [26], silica-based nanoparticles [27], iron-based materials [28], metal–organic frameworks [29], and biochar [30–32].

Biochar is a carbonaceous substance that is produced through the thermolysis (~700 °C) of various forms of biomass, including agricultural and forest residues, animal waste, and sludge, among others, in an environment that is either low in oxygen or completely devoid of it [33]. Biochar has a large specific surface area, abundant pore structure, numerous functional groups, good ion exchange ability, and good thermal stability. The physicochemical characteristics of biochar play a significant role in determining the surface interactions and adsorption mechanisms. Increasing the pyrolysis temperature enhances the characteristics of biochar, specifically its specific surface area and microporous structure, resulting in significant adsorption capabilities [34, 35].

There are studies on biochar obtained using walnut shells in the literature. However, the properties of walnut shell biochar (WSB) are affected by the raw material properties (type of walnut, climatic conditions in which it is grown, etc.), pyrolysis conditions (temperature, heating rate, residence time, etc.), and natural composition (moisture content, lignin, cellulose, and hemicellulose content, etc.) of walnut shells. In this study, biochar was obtained from the shells of Chandler-type walnuts grown in Burdur province, Turkey, using one- and two-step pyrolysis process at different temperatures (500, 600, 700, 700 + 700 °C). The biochar obtained was used as an adsorbent for naproxen removal from aqueous systems, and the WSB obtained by two-stage pyrolysis showed the highest removal efficiency (92%). Examination of the physicochemical attributes of the resulting walnut shell biochar (WSB) involved a comprehensive array of analytical techniques, including SEM (scanning electron microscopy), EDX (energy dispersive X-ray), BET (Brunauer–Emmett–Teller), XRD (X-ray diffraction), TGA (thermogravimetric analysis), and FTIR (Fourier transform iInfrared). Multiple experimental parameters, such as pH, initial naproxen concentration, adsorbent quantity, contact time, pHpzc, and temperature, were systematically investigated to gain insight into the naproxen adsorption process by WSB in aqueous solutions. The equilibrium results were analyzed using various adsorption isotherm models including the Langmuir, Sips, Temkin, and Freundlich models. Additionally, four adsorption kinetic models, pseudo-first-order (PFO), pseudo-second-order (PSO), Elovich, and intraparticle diffusion (IPD), were applied to characterize the adsorption kinetics. The thermodynamic parameters ($\Delta H^{\circ}$, $\Delta G^{\circ}$, and $\Delta S^{\circ}$) were determined to ascertain whether the adsorption process involved physical and/or chemical adsorption mechanisms. This comprehensive investigation aimed to elucidate the intricacies of the naproxen adsorption process onto WSB and its underlying thermodynamic and kinetic aspects.

## Materials and methods

### Materials

Naproxen sodium salt (≥ 98%), sodium hydroxide (≥ 98%), sodium chloride (99%), hydrochloric acid (37%), methyl alcohol (≥ 99.9%), acetonitrile (99%),

ethyl alcohol (≥ 99%) were obtained from Sigma Aldrich and utilised without additional purification.

### Production of walnut shells biochar

The walnut shells (WS) used in this study were sourced from Chandler walnut trees grown in the Karamanlı District of Burdur, Turkey. The peels separated from the fruit were washed several times with tap water and distilled water and dried at 70 °C for 48 h. The dried walnut shell residues were then pulverized using a ball mill, resulting in particles ranging from 0.16 to 0.25 mm in size. Walnut shell biochars were prepared by one- and two-step methods at different pyrolysis temperatures (500, 600, 700, 700 + 700 °C) [30]. Approximately 25 g of dried WS was placed in a porcelain crucible with a lid and then transferred to a muffle furnace. One-step pyrolysis was conducted at different temperatures (500, 600, 700 °C), 10 °C/min, and 4 h in a non-circulating air atmosphere. In the two-stage pyrolysis, this procedure was repeated twice. The biochar samples were thoroughly washed with distilled water until the filtrate attained a neutral value. Before being preserved in a desiccator for future use, the biochar was dried for 24 h at 80 °C to maintain a constant humidity.

### Characterization of walnut shell biochar

To assess the functional groups present in walnut shell biochar, Fourier transform infrared (FT-IR) spectra were recorded using a Perkin Elmer Frontier model spectrometer. A KBr pellet was used for the analysis, and the spectra were measured within the range of 500 to 4000 $cm^{-1}$. The thermal stability and mass loss properties of the walnut-shell biochar were determined using a Seiko SII TG/DTA 7200 thermal analyzer. LEO SEM-440-EDX was used to analyze the morphology and chemical composition of the biochar. A Bruker AXS D8 model X-Ray Diffraction equipment with a voltage of 40 kV, a current of 40 mA, and 2θ in the range of 10° to 90° was used to determine the crystal structure of the walnut shell biochar.

Nitrogen adsorption and desorption isotherm analyses were conducted using a surface characterization analyzer (Quantachrome Quadrasorb SI). Liquid nitrogen was used for the measurements, which were performed at a constant temperature of 77 K. Using a T60 UV–vis spectrophotometer (PG Instruments), the amount of naproxen in the aqueous solution was calculated. The point of zero charge (PZC) of the walnut shell biochar was determined using the common drift method [36]. In this method, a 25 mL solution of 0.1 M NaCl was mixed with approximately 50 mg of walnut shell biochar. Using 1 M NaOH or 1 M HCl, the pH of the solution (pH_initial) was varied from 2 to 12. An Orion 3 Star pH meter was used to measure the pH (pH_after) of the solutions after stirring the suspensions for 24 h at 25 °C and 120 rpm.

### Adsorption and desorption experiments

The adsorption capacity of walnut shell biochar for the selective removal of naproxen ions at room temperature was evaluated using a batch system. First, the ability of WSBs to remove naproxen from aqueous media at different pyrolysis temperatures was tested (Fig. S1). According to the results, naproxen removal rates were calculated as 700 + 700-WSB (92%) > 700-WSB (79%) > 600-WSB (28%) > 500-WSB (5%). Based on these results, 700 + 700-WSB was selected as the adsorbent to remove naproxen from aqueous media because it exhibited the best removal efficiency.

Several crucial parameters were investigated to optimize the adsorption process for naproxen removal from water samples. These parameters included pH values ranging from 5.0 to 8.0, contact times from 0 to 300 min, different amounts of adsorbent (0–2 g/L), varying initial naproxen concentrations (10–400 mg/L), and temperatures of 25 °C, 40 °C, and 55 °C. The pH of the aqueous solution plays a remarkable role in the adsorption of naproxen. The pH of the samples was adjusted within the range of 5.0–8.0, while keeping other experimental conditions constant, such as the amount of 700 + 700-WSB (2 g/L), naproxen concentration (10 mg/L), temperature (25 °C), and contact time (4 h). To examine the adsorption equilibrium, a range of initial naproxen concentrations (10–400 mg/L) were investigated at various temperatures (25, 40, and 55 °C) over a duration of 4 h. The adsorption kinetics study was conducted at 25 °C for contact times ranging from 10 to 300 min. Filtration was used to separate the solid–liquid mixture after the adsorption process was completed. Using a PG Instruments T60 Model UV–vis spectrophotometer, the absorbance data at a wavelength of 232 nm were used to calculate the amount of naproxen in the solution. The R% (removal efficiency), quantity of naproxen adsorption Qt (mg/g) at a specific time, and quantity of naproxen adsorbed at equilibrium Qe (mg/g) were calculated using Eq. (1)-(3). By conducting these experiments and analyzing the data, valuable insights were gained regarding the optimal conditions for naproxen removal and the adsorption characteristics of walnut shell biochar.

$$R\% = \frac{C_0 - C_t}{C_0} \times 100 \tag{1}$$

$$Q_t = \frac{C_0 - C_t}{m} \times V \tag{2}$$

$$Q_e = \frac{C_0 - C_e}{m} \times V \tag{3}$$

here $C_0$ (mg/L), $C_e$ (mg/L), and $C_t$ (mg/L) represent the initial ion concentration, equilibrium ion concentration, and ion concentration in the liquid phase at any given time. V (L) represents the volume of the ion solution and m (g) represents the total amount of adsorbent used. The results of the triple adsorption studies are presented as the mean value and standard deviation (SD). A non-linear optimization technique was utilized to obtain the relevant variables of the models employed in

the adsorption isotherm and kinetics. The ishoterm and kinetic model equations and parameters used are listed in Tables S1 and S2.

After the adsorption investigation with 10 mg/L of naproxen, 2 g/L adsorbents, pH 6.8, and 25 °C was completed, the solution was filtered. The 700 + 700-WSB adsorbent was washed with distilled water and dried at 60 °C for 12 h for desorption. For the desorption of naproxen adsorbed on 700 + 700-WSB, various desorption agents including acetonitrile, methanol, ethanol, 0.5 mol/L NaOH and, 0.5 mol/L HCl were utilized. 700 + 700-WBS@Naproxen (50 mg naproxen-loaded WBSs) was used for the desorption investigation, which was conducted using 25 mL of each desorbing agent for 4 h. The solutions were then filtered through filter paper and a UV spectrometer was used to measure the resulting naproxen concentrations.

### Adsorption data modeling

In this study, the experimental equilibrium data were fitted with the Langmuir [37], Sips [38], Temkin [39] and, Freundlich [40] mathematical models. Table S1 contains all isotherm model equations and parameters. In addition, PFO [41], PSO [42], Elovich [43] and IPD [44] models were used to fit the kinetic experimental data. Table S2 contains all kinetic model equations and parameters.

## Results and discussion

### Characterization of walnut shell biochar

The pH of the solution has a significant impact on the surface charge of each adsorbent. The point at which the positive charge density on the surface of the adsorbent is equal to the negative charge density is known as the point of zero charge (PZC) of the material in solution (Fig. S2a). To understand the effect of pH on the adsorption behaviour, it is very important to know the $pH_{pzc}$ of the adsorbent. Based on this methodology, the superior adsorption of cations occurs at a pH level greater than the $pH_{pzc}$, whereas the enhanced adsorption of anions transpires at a pH level lower than $pH_{pzc}$. The pKa value of naproxen (Fig. S2b) is approximately 4.19 [7, 45], indicating that naproxen exists predominantly in its anionic form when the solution pH exceeds its pKa value. Calculation of the point of zero charge ($pH_{pzc}$) for the 700 + 700-WSB adsorbent yielded a value of 7.15. It is hypothesized that electrostatic attraction plays a more significant role in the adsorption of naproxen on WSB than other interactions (such as pore filling, π-π interactions, and hydrogen bonding) when the pH is lower than $pH_{pzc}$.

The FTIR spectrum of the 700 + 700-WSB and 700 + 700-WSB@Naproxen showed some well-defined bands (Fig. 1a). The prominent functional group vibrations of 700 + 700-WSB and 700 + 700-WSB@Naproxen included ν O–H or N–H (3440, 3437 cm-1), $\nu_{as}$ C-H (2923 $cm^{-1}$), ν C-H (2850 $cm^{-1}$), ν C=O (1646 $cm^{-1}$), ν C=C (1543 $cm^{-1}$), and aromatic ν C–O (1211, 1208 $cm^{-1}$) [31, 35, 46–48]. According to FTIR analysis before and after the adsorption process,

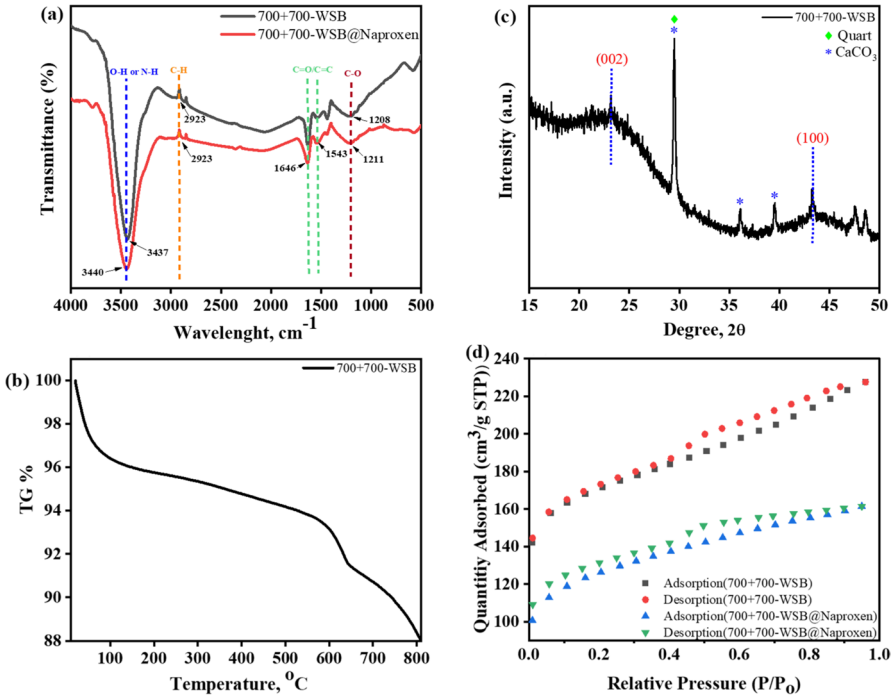


**Fig. 1** **a** FTIR spectra of 700 + 700-WSB before and after naproxen adsorption; **b** TG curve of 700 + 700-WSB; **c** XRD patterns of 700 + 700-WSB; **d** Nitrogen adsorption isotherms of 700 + 700-WSB before and after naproxen adsorption

no new characteristic peaks associated with naproxen molecules were observed in the FTIR spectra after the adsorption of naproxen on the WSBs. This suggests that the adsorption process was based on physical interactions.

The TGA curve of 700 + 700-WSB is given in Fig. 1b. The initial phase of weight reduction was observed within the temperature range of the ambient temperature to 130 °C, which was primarily attributed to the process of moisture evaporation. The weight loss in the temperature range of 140–650 °C was due to the thermal decomposition of hemicellulose (225–350 °C), cellulose (325–375 °C), and lignin (250–500 °C) structures [49–51]. The total mass loss of the 700 + 700-WSB was calculated to be 12%.

The XRD technique was applied to determine the amorphous structure of the 700 + 700-WSB, as shown in Fig. 1c. The diffraction peak at approximately 23° (002) represents the layer spacing and thickness of the aromatic microcrystalline structure, while the diffraction peak at 43° (100) represents the size of the aromatic layer [50, 52, 53]. Furthermore, the additional peaks that were observed could potentially pertain to the diverse inorganic constituents present in the input material, such as feasible quart, and calcite minerals [30]. The measured diffraction peaks correspond to the standard diffraction pattern of JCPDS card file number 01–089-1304 [54].

The 700 + 700-WSB and 700 + 700-WSB@Naproxen $N_2$ adsorption–desorption isotherms are shown in Fig. 1d, and the pore size distribution is shown in Fig. S3. As can be seen from Fig. 1d, the 700 + 700-WSB adsorbent exhibited an IV-type isotherm and a mesoporous hysteresis loop type H4. The adsorption behavior within the mesopores and micropores is influenced by the interactions between the adsorbent and adsorbate as well as the interactions among molecules in the condensed phase [55, 56]. According to Table 1, the micropore volume ($V_{micro}$) comprises a greater proportion of the total pore volume than the mesopore volume ($V_{meso}$). The surface areas of 700 + 700-WSB before and after adsorption were calculated as 649.9 and 469.5 $m^2/g$, respectively. The decrease in the surface area and pore volumes of 700 + 700-WSB before and after adsorption suggests that naproxen adsorption occurs both on the surface and in the form of pore filling.

The macropores and mesopores shown in Fig. 2 facilitate the diffusion of numerous naproxen molecules into the pore structure. The results presented in Fig. 2 show that naproxen adsorption leads to alterations in the surface morphology, causing disruption of the cavities and pores. The surface porosity of 700 + 700-WSB became less visible, indicating that naproxen molecules were adsorbed onto the surface through functional groups until these groups became saturated. After saturation, naproxen molecules penetrate deeply into the porous structure of the WSB and are adsorbed onto the inner surfaces of the pores.

EDX analysis indicated that the 700 + 700-WSB adsorbent has a high carbon content, aligning well with the findings from XRD analysis. The elemental analysis presented in Fig. S4 reveals that the 700 + 700-WSB sample consists of approximately 85.64% carbon and 11.81% oxygen prior to naproxen adsorption. Fig. S5 displays the EDX spectrum and data of the 700 + 700-WSB sample after adsorption. The rise in oxygen percentage to 12.94% in the 700 + 700-WSB sample suggests successful naproxen adsorption onto the sample.

## Factors affecting naproxen adsorption

The impact of 700 + 700-WSB on the adsorption capacity of naproxen was examined at different pH levels, and the findings from the experiment are shown in Fig. S6. In the studies carried out in the range of pH 5.0–8.0, the highest naproxen adsorption

**Table 1** Textural information of the 700 + 700-WSB and 700 + 700-WSB@Naproxen

| | Symbol | Unite | 700 + 700-WSB | 700 + 700-WSB@Naproxen |
|---|---|---|---|---|
| BET | $S_{BET}$ | $m^2/g$ | 649.9 | 469.5 |
| Total pore | $V_{Total}$ | $cm^3/g$ | 0.352 | 0.248 |
| Micropore | $V_{Micro}$ | $cm^3/g$ | 0.248 | 0.184 |
| Mesopore | $V_{Mezo}$ | $cm^3/g$ | 0.104 | 0.064 |
| Average pore width | $L_o$ | nm | 1.083 | 1.064 |

$C_o$ of naproxen: ~ 500 mg/L

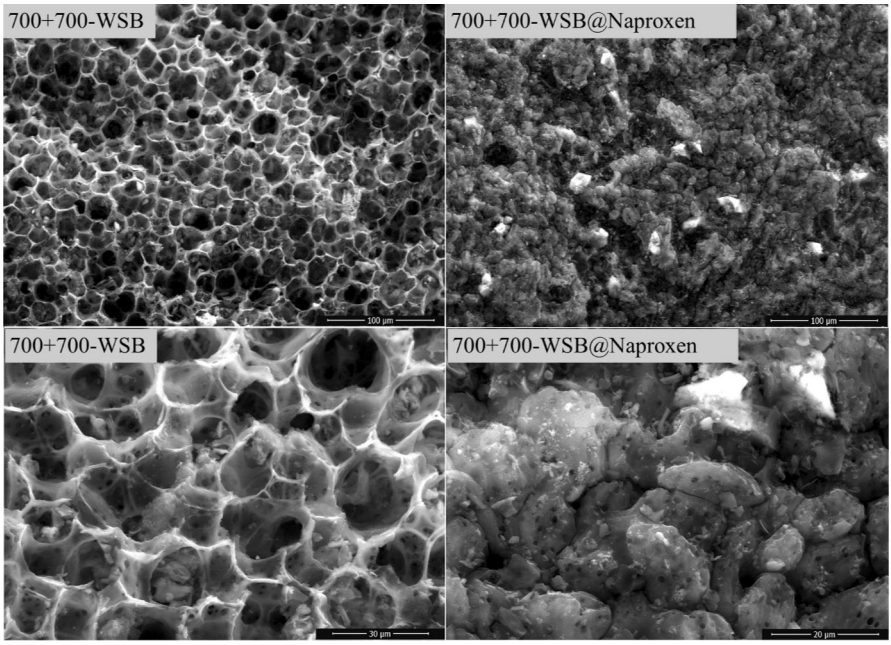


**Fig. 2** SEM images of the 700 + 700-WSB surface before (1000x, 3000x) and after (1000x, 5000x) Naproxen adsorption at two different magnifications

removal of 700 + 700-WSB was obtained at pH 6.84 (% 92). In Sect. "Characterization of walnut shell biochar", it is stated that the pKa value of naproxen is approximately 4.19 and, in this case, naproxen is found in anionic form when the solution pH is higher than its pKa. In this case, the process of adsorption takes place between the anions of naproxen present in the solution and the positively charged surface of biochar, primarily because of mutual electrostatic attraction. At pH 6.84, where the highest removal occurs, naproxen is in the anionic form, and the surface charge of 700 + 700-WSB is positive at this pH value. A decrease in naproxen removal was observed when the pH was 8.0, because the surface charge of the 700 + 700-WSB was negative. For this reason, pH 6.84 was chosen as the optimum pH value for naproxen adsorption on 700 + 700-WSB.

The effect of the amount of adsorbent on the percentage removal of naproxen molecules is shown in Fig. S7. As shown in Fig. S7, the percentage of naproxen removal increased simultaneously with an increase in the adsorbent amount. This is due to the increased surface area and active sites resulting from the increase in adsorbent amount. In addition, because the highest removal percentage was obtained at 2 g/L (92%), this was determined to be the optimum adsorbent amount in naproxen adsorption studies**.**

The time dependence of naproxen adsorption on WSB was investigated using an initial naproxen concentration of 10 mg/L (Fig. S8). The data in Fig. S8 show that there is an increase in removal up to approximately 240 min, but no significant increase in the removal percentage was observed after 240 min, and the equilibrium

state was reached. When the results were evaluated, 240 min was determined to be the optimum time for naproxen adsorption on WSB.

To investigate the temperature dependence of naproxen adsorption on WSB, adsorption studies were conducted at three different temperatures (25, 40, and 55 °C). As shown in Fig. S9, the highest removal efficiency was achieved at room temperature (25 °C, 92%).

## Adsorption kinetics

Adsorption kinetics is an important parameter in explaining the adsorption properties of an adsorbent. Kinetic experiments were conducted at room temperature and the natural pH of the solution (pH 6.84) using a 10 mg/L concentration of naproxen and 2 g/L of 700 + 700-WSB over a range of 0–300 min. In this study, the adsorption kinetics were explained by PFO, PSO, Elovich, and intraparticle diffusion models. The kinetic curves of naproxen adsorption by the WSBs at an initial concentration of 10 mg/L are shown in Fig. 3a, and the corresponding parameters of the applied models are listed in Table 2. When Table 2 is analyzed, the $R^2$ values for the PFO, PSO, and Elovich models were 0.989, 0.998, and 0.993. Considering the $R^2$ values, it can be seen that the most compatible model was PSO. However, the qe value (4.53 mg/g) obtained in the PFO model is closer to the value obtained with the experimental data (4.62 mg/g). Therefore, the intraparticle diffusion process should be examined to better define the adsorption mechanism.

Generally, adsorption occurs in three stages: film diffusion, surface diffusion, and intraparticle diffusion. Film diffusion initially occurs as the adsorbate is transported to the surface of the adsorbent. In the second stage, the adsorbate molecules penetrated the interior of the particles through intraparticle diffusion. Finally, adsorption of the adsorbate occurs in the active regions of the internal and external surfaces, leading to a final equilibrium stage. This equilibrium stage is reached when the intraparticle diffusion process slows down owing to the very low residual adsorbate concentration and decrease in available adsorption sites [44, 57]. If the curve

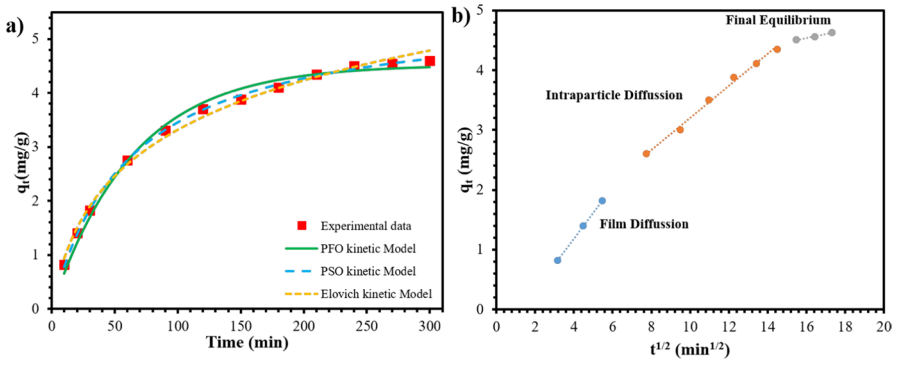


**Fig. 3** **a** PFO, PSO and Elovich kinetics for naproxen adsorption onto 700 + 700-WSB, **b** Intra particle diffusion mechanism for naproxen adsorption onto 700 + 700-WSB. (adsorption conditions: 2 g/L 700 + 700-WSB, 10 mg/L naproxen, 25 °C, pH = 6.84, 5 h)

**Table 2** Corresponding parameters for naproxen adsorption onto 700 + 700-WSB in the kinetic models

| Model Parameters | | Unit | Initial Naproxen concentration 10 mg/L |
|---|---|---|---|
| PFO | $q_e$ | mg/g | 4.534 ± 0.081 |
| | $k_1(\times 10^{-2})$ | 1/min | 1.548 ± 0.057 |
| | $R^2$ | – | 0.989 |
| PSO | $q_e$ | mg/g | 5.583 ± 0.178 |
| | $k_2(\times 10^{-3})$ | g/(mg • min) | 2.912 ± 0.043 |
| | $R^2$ | – | 0.998 |
| Elovich | α | g/(mg • min) | 0.132 ± 0.018 |
| | β | mg/g | 0.701 ± 0.083 |
| | $R^2$ | – | 0.993 |
| | $k_{int}$ | mg/(g.min$^{1/2}$) | 0.267 ± 0.015 |
| Intra-particle diffusion | C | mg/g | 0.527 ± 0.216 |
| | $R^2$ | – | 0.993 |

representing intraparticle diffusion is drawn such that it passes through the origin, intraparticle diffusion will be the only factor limiting the adsorption rate. However, Fig. 3b shows the presence of a three-step linear region; therefore, the adsorption process is controlled by a multistep mechanism. The first linear part of Fig. 4b ($3.162 \leq t_{0.5} \leq 5.477$) shows the liquid film diffusion step. This linear region represents the outer mass transfer from the solution to the outer surface of the 700 + 700-WSB. The second linear part ($7.745 \leq t0.5 \leq 14.491$) represents intra-particle diffusion, which means binding of adsorbate to the pores of 700 + 700-WSB active sites. The third phase signifies the attainment of the final equilibrium stage, wherein intraparticle diffusion decelerates owing to the low remaining adsorbate concentration and the reduced availability of adsorption sites on the surface of the 700 + 700-WSB.

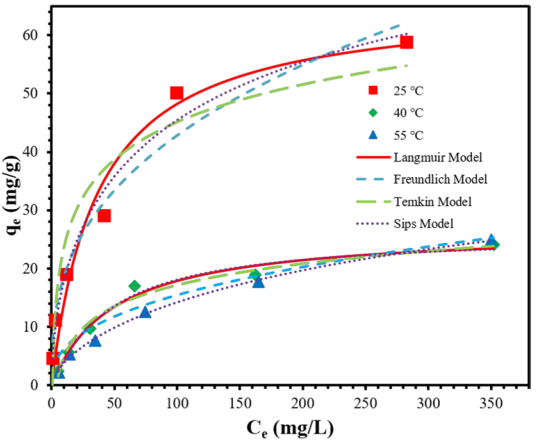


**Fig. 4** At various solution temperatures, the isotherm of naproxen adsorption onto the 700 + 700-WSB adsorbent. (adsorption conditions: 2 g/L 700 + 700-WSB, initial naproxen concentration 10–400 mg/L, pH = 6.84, 4 h)

Hence, the presence of multicollinearity in the graph suggests that the adsorption of naproxen on 700 + 700-WSB involves not only intraparticle diffusion, but also external mass transfer [44, 58].

## Adsorption isotherms

Isotherm tests were conducted in 240 min at three distinct temperatures—25, 40, and 55 °C—and at the solution's natural pH of 6.84 using a ratio of 2 g/L 700 + 700-WSB and a concentration range of 10–400 mg/L naproxen. To predict the naproxen adsorption mechanisms on WSB, equilibrium data were used for the nonlinear Langmuir, Sips, Temkin and, Freundlich, isotherm models (Fig. 4). The corresponding model parameters are listed in Table 3.

Langmuir isotherm theory [37] posits that adsorbate molecules are adsorbed onto a morphologically uniform adsorbent surface in a single layer. This surface contains a fixed number of energetically equivalent adsorption sites that do not interact laterally. In contrast to Langmuir's model, the Freundlich model [40] suggests the existence of active sites with varying energies on a heterogeneous surface and proposes that adsorption occurs in multiple layers. The Sips isotherm model [59] is a composite model that integrates Freundlich and Langmuir isotherms. It is commonly employed in heterogeneous adsorption situations, in which the adsorbed molecule exhibits multiple adsorption sites. However, the current model fails to consider the potential synergistic effects between adsorbates. During the adsorption process, the Temkin adsorption model [60] accounts for the indirect interaction between the adsorbent and adsorbate. In addition, this model accounts for the coverage of a single layer. Assuming that the adsorption heat decreases linearly, rather than logarithmically, this model concludes that

**Table 3** Corresponding isotherm parameters for naproxen adsorption onto 700 + 700-WSB at different temperatures

| Model Parameters | | Unit | Solution temperature | | |
|---|---|---|---|---|---|
| | | | 25°C | 40°C | 55°C |
| Langmuir | $q_{max}$ | mg/g | 58.873 ± 3.641 | 31.592 ± 2.582 | 26.761 ± 1.627 |
| | $K_L$ | L/mg | 0.027 ± 0.002 | 0.020 ± 0.001 | 0.009 ± 0.003 |
| | $R^2$ | – | 0.984 | 0.985 | 0.982 |
| Freundlich | $K_F$ | $(mg/g)\cdot(mg/L)^n$ | 8.225 ± 2.647 | 2.528 ± 0.877 | 1.391 ± 0.188 |
| | n | – | 0.358 ± 0.069 | 0.495 ± 0.025 | 0.392 ± 0.066 |
| | $R^2$ | – | 0.966 | 0.983 | 0.966 |
| Temkin | B | J/mol | 9.286 ± 1.293 | 5.367 ± 0.188 | 5.320 ± 0.407 |
| | $K_T$ | L/mg | 1.287 ± 0.669 | 0.185 ± 0.025 | 0.251 ± 0.054 |
| | $R^2$ | – | 0.927 | 0.953 | 0.977 |
| Sips | $K_S$ | L/g | 0.058 ± 0.001 | 0.017 ± 0.003 | 0.015 ± 0.004 |
| | $q_{ms}$ | - | 98.927 ± 4.517 | 58.169 ± 1.348 | 25.934 ± 2.978 |
| | *m* | – | 0.582 ± 0.023 | 0.664 ± 0.125 | 1.066 ± 0.205 |
| | $R^2$ | – | 0.979 | 0.997 | 0.983 |

the adsorbate adheres to the adsorbent and covers its surface. This model considers the interceding ion concentrations. An exothermic adsorption process is indicated by a positive value of parameter B, whereas an endothermic process is indicated by a negative value of parameter B.

From Fig. 4, it can be seen that the isotherm data for none of the three temperatures fits the Freundlich isotherm. Furthermore, the values of $n < 1$, as presented in Table 3, suggest that the adsorption process was unsuitable for multilayer adsorption. In addition, the highest $R^2$ values in Table 3 correspond to the Langmuir (0.985) and Sips (0.997) models. The fact that the Sips heterogeneity constant m is close to 1 indicates that naproxen adsorption follows a Langmuir-like isotherm model, and that adsorption occurs on a homogeneous surface. It was also found that naproxen adsorption on 700 + 700-WSB was more consistent with the Langmuir isotherm when the experimental $q_{max}$ value (58.307 mg/g) was compared to the calculated $q_{max}$ value (58.873 mg/g). The positive B value obtained from the Temkin isotherm model for naproxen adsorption on 700 + 700-WSB indicates that adsorption is exothermic and spontaneous.

## Adsorption thermodynamics

An essential stage in the investigation of adsorption processes is the accurate determination of the thermodynamic parameters. An effective method for evaluating the thermodynamic variables involved in an adsorbate/adsorbent system is based on the application of the reaction equilibrium constant. In this study, the temperature dependence of naproxen uptake by 700 + 700-WSB was investigated in the range 25–55 °C. The thermodynamic parameters, enthalpy change ($\Delta H°$), Gibbs free energy ($\Delta G^o$), and entropy change ($\Delta S°$), were calculated using Eq. 4:

$$\ln K_C = \frac{-\Delta H^\circ}{R} \times \frac{1}{T} + \frac{\Delta S^\circ}{R} \tag{4}$$

$$K_C \approx K_L \times M_{\text{Naproxen}} \times C^O \times \left(10^3\right) \tag{5}$$

here $K_C$ is the dimensionless equilibrium constant, R is the universal constant for gases (8.314 J/mol K), where T is the absolute temperature in Kelvin (K). To determine the thermodynamic characteristics of the naproxen adsorption process on 700 + 700-WSB, $K_L$ (Langmuir constant) was used. $K_L$ was converted to $K_C$ using Eq. 5 [30].

The negative $\Delta G°$ and $\Delta H°$ values in Table 4 indicate that the adsorption of naproxen on the WSBs occurs spontaneously and exothermically. Furthermore, the negative $\Delta H°$ (− 29.52 kJ/mol) value indicates that the adsorption of naproxen by WSBs is weak interactions may play a role in adsorption [36]. The negative entropy value ($\Delta S^o = -0.026$ kJ/mol K) indicates that randomness decreases after the uptake of naproxen by 700 + 700-WSB [61].

**Table 4** Thermodynamic parameters obtained from the adsorption of naproxen by the WSB adsorbent

| T (K) | $K_C$ | Van't Hoff equation | $\Delta G°$ (kJ/mol) | $\Delta H°$ (kJ/mol) | $\Delta S°$ (kJ/mol K) |
|---|---|---|---|---|---|
| 298 | 6217 ± 460 | y = 3551.3x -3.0946<br>$R^2$ = 0.922 | − 21.85 ± 0.057 | − 29.52 ± 8 | − 0.026 ± 0.002 |
| 313 | 4605 ± 230 | | − 21.47 ± 0.421 | | |
| 328 | 2072 ± 196 | | − 21.08 ± 0.788 | | |

## Desorption, reusability, and potential real sample application

Desorption is a crucial factor in prospective environmental applications in terms of sustainability and economic effectiveness. According to the literature, alcohol hydroxyl groups provide them with higher solubility for organic micropollutants [36, 62].

As shown in Table 5, ethanol (68%) and methanol (59%) were the most effective desorption agents for naproxen. Other desorption agents (acetonitrile, NaOH, HCl and pH = 12 distilled water) were not as effective as ethanol and methanol in naproxen desorption. In general, however, the desorption efficiency was relatively low under the desorption agents used. This suggests a large contribution of pore filling as well as weak interaction in the adsorption mechanism.

The reusability of 700 + 700-WSB was tested using the data obtained from three adsorption–desorption cycles (Fig. S10). Ethanol, which provided the highest desorption efficiency, was used as the desorption agent. The adsorption–desorption operating conditions were as follows: room temperature, 2 g/L 700 + 700-WSB, 10 mg/L naproxen concentration, and 4 h. It was observed that 700 + 700-WSB retained more than 75% of its initial adsorption capacity after three adsorption/desorption cycles.

To validate naproxen adsorption using the 700 + 700-WSB adsorbent, a real sample study was conducted with four different water samples. In Table 6, the amount of naproxen spiked into the real water samples and the % removal are given. For naproxen, the removal percentages obtained in real water samples were lower than those in the model solutions (92%). This may be due to competitive adsorption between atomic (i.e. $Na^+$, $K^+$, $Cl^-$) and/or molecular species

**Table 5** Desorption efficiency (%) of naproxen from the 700 + 700-WSB (Desorption conditions, $C_o$ = 10 mg/L, 4 h, 25 °C, 2 g/L)

| Desorption agents | Desorption efficiency (%) |
|---|---|
| Ethanol | 68 ± 2 |
| Methanol | 59 ± 3 |
| Acetonitrile | 32 ± 1 |
| 0.5 M NaOH | 31 ± 1 |
| pH = 12 Distilled water | 10 ± 2 |
| 0.5 M HCl | 8 ± 1 |

**Table 6** The adsorption removal of naproxen onto the 700 + 700-WSB adsorbent under different water matrices

| Sample | Spiked, mg/L | Found, mg/L | % Removal |
|---|---|---|---|
| Drinking water | – | – | – |
| | 1 | 0.23 ± 0.08 | 77 ± 1 |
| | 2 | 0.44 ± 0.10 | 78 ± 2 |
| Tap water | – | – | – |
| | 1 | 0.25 ± 0.03 | 75 ± 1 |
| | 2 | 0.45 ± 0.15 | 78 ± 3 |
| Waste water (1) | – | – | – |
| | 1 | 0.24 ± 0.02 | 76 ± 1 |
| | 2 | 0.43 ± 0.05 | 79 ± 1 |
| Waste water (2) | – | – | – |
| | 1 | 0.39 ± 0.05 | 61 ± 1 |
| | 2 | 0.81 ± 0.17 | 60 ± 2 |

95% confidence level, N = 3

(i.e. $NO^{2-}$) or uncharged species and naproxen ions, which are present at different concentrations in real water samples as binding sites in the structure of WSBs.

## Conclusions

In this study, biochar was obtained from walnut shells (WS) using a one and two-stage pyrolysis process. The obtained biochars was used as an adsorbent for the removal of naproxen, an organic pollutant, from aquatic systems. When the naproxen removal efficiency of the synthesized biochars from aqueous systems was examined, it was determined that 700 + 700-WSB obtained by two-stage pyrolysis had the highest removal efficiency (92%). Walnut shell biochar (700 + 700-WSB) had a high surface area of 649 $m^2$/g and pronounced porous structure according to BET and SEM analysis results. The highest amount of naproxen removed, as determined by adsorption studies, was 58.8 mg/g. While the $pH_{PZC}$ for 700 + 700-WSB was at pH 7.15, the greatest adsorption efficiency was observed at neutral pH (6.84), indicating the involvement of electrostatic attraction in adsorption. The adsorption of naproxen on 700 + 700-WSB was in good agreement with the Langmuir and Sips isotherm models, with removal capacities of 58.87 and 98.92 mg/g were obtained. However, while the adsorption of naproxen on WSB is adapted to the PSO kinetic model, the adsorption process is controlled by a multi-step mechanism. The thermodynamic results revealed that the adsorption process was exothermic and spontaneous. In Table S3, the naproxen adsorption capacities of 700 + 700-WSB and the other adsorbents are compared. Various water samples were subjected to adsorption, and satisfactory results were obtained. In conclusion, 700 + 700-WSB is an effective adsorbent for naproxen removal.

**Supplementary Information** The online version contains supplementary material available at https://doi.org/10.1007/s11144-024-02586-1.

**Acknowledgements** This research was supported by the Fundamental Research Funds of Burdur Mehmet Akif Ersoy University under the project number of 0652-YL-20.

**Author contributions** RŞ: Investigation, Visualization, Data curation, Formal analysis, Writing– original draft. BK: Investigation, Visualization, Data curation, Formal analysis, Writing—original draft. EK: Conceptualization, Methodology, Formal analysis, Investigation, Resources, Writing—original draft, Writing—review & editing, Visualization, Supervision, Project administration, Funding acquisition.

**Data Availability** Data will be made available on request.

## Declarations

**Competing interest** The authors have no conflict of interest.

## References

1. Tu N, Liu Y, Li R, Lv W, Liu G, Ma D (2019) Experimental and theoretical investigation on photodegradation mechanisms of naproxen and its photoproducts. Chemosphere 227:142–150. https://doi.org/10.1016/j.chemosphere.2019.04.055
2. Wieszczycka K, Zembrzuska J, Bornikowska J, Wojciechowska A, Wojciechowska I (2017) Removal of naproxen from water by ionicliquid-modified polymer sorbents. Chem Eng Res Des 117:698–705. https://doi.org/10.1016/j.cherd.2016.11.024
3. Afkhami A, Kafrashi F, Ahmadi M, Madrakian T (2015) A new chiral electrochemical sensor for the enantioselective recognition of naproxen enantiomers using L-cysteine self-assembled over gold nanoparticles at gold electrode. RSC Adv 5:58609–58615. https://doi.org/10.1039/C5RA07396K
4. Madikizela LM, Chimuka L (2016) Synthesis, adsorption and selectivity studies of a polymer imprinted with naproxen, ibuprofen and diclofenac. J Environ Chem Eng 4:4029–4037. https://doi.org/10.1016/j.jece.2016.09.012
5. Vulava VM, Cory WC, Murphey VL, Ulmer CZ (2016) Sorption, photodegradation, and chemical transformation of naproxen and ibuprofen in soils and water. Sci Total Environ 565:1063–1070. https://doi.org/10.1016/j.scitotenv.2016.05.132
6. Nodeh MKM, Kanani N, Abadi EB, Sereshti H, Barghi A, Rezania S, Bidhendi GN (2021) Equilibrium and kinetics studies of naproxen adsorption onto novel magnetic graphene oxide functionalized with hybrid glycidoxy-amino propyl silane. Environ Chall 4:100106. https://doi.org/10.1016/j.envc.2021.100106
7. Xing L, Haddao KM, Emami N, Nalchifard F, Hussain W, Jasem H, Dawood AH, Toghraie D, Hekmatifar M (2022) Fabrication of HKUST-1/ZnO/SA nanocomposite for doxycycline and naproxen adsorption from contaminated water. Sustain Chem Pharm 29:100757. https://doi.org/10.1016/j.scp.2022.100757
8. Organization, W.H. (2012) Pharmaceuticals in Drinking-Water. https://apps.who.int/iris/handle/10665/44630
9. Kurtulbaş E, Bilgin M, Şahin S, Bayazit ŞS (2017) Comparison of different polymeric resins for naproxen removal from wastewater. J Mol Liq 241:633–637. https://doi.org/10.1016/j.molliq.2017.06.070
10. Czech B, Kończak M, Rakowska M, Oleszczuk P (2021) Engineered biochars from organic wastes for the adsorption of diclofenac, naproxen and triclosan from water systems. J Clean Prod 288:125686. https://doi.org/10.1016/j.jclepro.2020.125686
11. Al-Qaim FF, Mussa ZH, Yuzir A, Abdullah MP, Othman MR (2018) Removal of pharmaceutically active compounds from wastewater using adsorption coupled with electrochemical oxidation technology: a critical review. J Braz Chem Soc 29:1721–1731. https://doi.org/10.21577/0103-5053.20180047

12. Matin A, Jillani SMS, Baig U, Ihsanullah I, Alhooshani K (2023) Removal of pharmaceutically active compounds from water sources using nanofiltration and reverse osmosis membranes: comparison of removal efficiencies and in-depth analysis of rejection mechanisms. J Environ Manage 338:117682. https://doi.org/10.1016/j.jenvman.2023.117682
13. Shirafkan A, Nowee SM, Ramezanian N, Etemadi MM (2016) Hybrid coagulation/ozonation treatment of pharmaceutical wastewater using ferric chloride, polyaluminum chloride and ozone. Int J Environ Sci Technol 13:1443–1452. https://doi.org/10.1007/s13762-016-0965-8
14. Muniozguren PA, Galvis EAS, Bussemaker M, Palma RAT, Lee J (2021) A review on pharmaceuticals removal from waters by single and combined biological, membrane filtration and ultrasound systems. Ultrason Sonochem 76:105656. https://doi.org/10.1016/j.ultsonch.2021.105656
15. Kanakaraju D, Glass BD, Oelgemöller M (2014) Titanium dioxide photocatalysis for pharmaceutical wastewater treatment. Environ Chem Lett 12:27–47. https://doi.org/10.1007/s10311-013-0428-0
16. Bambague EMJ, Arias DSV, Vanegas ODR, Gómez DDG, Parra CAM, Salamanca EJP, Filho CRM, Martínez FM (2023) Removal of pharmaceutical compounds from real urban wastewater by a continuous bio-electrochemical process at pilot scale. J Environ Chem Eng 11:110130. https://doi.org/10.1016/j.jece.2023.110130
17. Chen W, Xu J, Lu S, Jiao W, Wu L, Chang AC (2013) Fates and transport of PPCPs in soil receiving reclaimed water irrigation. Chemosphere 93:2621–2630. https://doi.org/10.1016/j.chemosphere.2013.09.088
18. Qin Z, Liu S, Liang SX, Kang Q, Wang J, Zhao C (2016) Advanced treatment of pharmaceutical wastewater with combined micro-electrolysis, fenton oxidation, and coagulation sedimentation method. Desalin Water Treat 57:25369–25378. https://doi.org/10.1080/19443994.2016.1155174
19. Bambague EMJ, Parra CAM, Delgado MFR, Martinez IQ, Mosquera DM, Apolinar JSA, Martínez FM (2023) Photo-fenton and electro-fenton performance for the removal of pharmaceutical compounds in real urban wastewater. Electrochim Acta 442:141905. https://doi.org/10.1016/j.electacta.2023.141905
20. Pereira D, Gil MV, Esteves VI, Silva NJO, Otero M, Calisto V (2023) Ex-situ magnetic activated carbon for the adsorption of three pharmaceuticals with distinct physicochemical properties from real wastewater. J Hazard Mater 443:130258. https://doi.org/10.1016/j.jhazmat.2022.130258
21. Cao Y, Li X, Wang B (2022) Ultrafast and selective adsorption of pharmaceuticals from wastewater by precisely designed metal organic framework with missing linker defects. J Clean Prod 380:135060. https://doi.org/10.1016/j.jclepro.2022.135060
22. Xiong P, Zhanga H, Li G, Liao C, Jiang G (2021) Adsorption removal of ibuprofen and naproxen from aqueous solution with Cu-doped Mil-101(Fe). Sci Total Environ 797:149179. https://doi.org/10.1016/j.scitotenv.2021.149179
23. Tran HN, Nguyen HC, Woo SH, Nguyen TV, Vigneswaran S, Bandegharaei AH, Rinklebe J, Sarmah AK, Ivanets A, Dotto GL, Bui TT, Juang RS, Chao HP (2019) Removal of various contaminants from water by renewable lignocellulose-derived biosorbents: a comprehensive and critical review. Crit Rev Environ Sci Technol 49:2155–2219. https://doi.org/10.1080/10643389.2019.1607442
24. Rac V, Rakicà V, Stošić D, Pavlović V, Bosnar S, Auroux A (2020) Enhanced accessibility of active sites in hierarchical ZSM-5 zeolite for removal of pharmaceutically active substances: adsorption and microcalorimetric study. Arab J Chem 13:1945–1954. https://doi.org/10.1016/j.arabjc.2018.02.012
25. Thiebaulta T, Boussafira M, Fougèrec L, Destandauc E, Monnina L, Le Milbeaua C (2019) Clay minerals for the removal of pharmaceuticals: Initial investigations of their adsorption properties in real wastewater effluents. Environ Nanotechnol Monit Mana 12:100266. https://doi.org/10.1016/j.enmm.2019.100266
26. El-Sheikh AH, Qawariq RF, Abdelghani JI (2019) Adsorption and magnetic solid-phase extraction of NSAIDs from pharmaceutical wastewater using magnetic carbon nanotubes: effect of sorbent dimensions, magnetite loading and competitive adsorption study. Environ Technol Innov 16:100496. https://doi.org/10.1016/j.eti.2019.100496
27. Subaihi A, Shahat A (2023) Synthesis and characterization of super high surface area silica-based nanoparticles for adsorption and removal of toxic pharmaceuticals from aqueous solution. J Mol Liq 378:121615. https://doi.org/10.1016/j.molliq.2023.121615
28. Olusegun SJ, Souza TGF, Souza GO, Osial M, Mohallem NDS, Ciminelli VST, Krysinski P (2023) Iron-based materials for the adsorption and photocatalytic degradation of pharmaceutical drugs: a

comprehensive review of the mechanism pathway. J Water Process Eng 51:103457. https://doi.org/10.1016/j.jwpe.2022.103457
29. Zhao F, Fang S, Gao Y, Bi J (2022) Removal of aqueous pharmaceuticals by magnetically functionalized Zr-MOFs: Adsorption Kinetics, Isotherms, and regeneration. J Colloid Interface Sci 615:876–886. https://doi.org/10.1016/j.jcis.2022.02.018
30. Tomul F, Arslan Y, Kabak B, Trak D, Kendüzler E, Lima EC, Tran HN (2020) Peanut shells-derived biochars prepared from different carbonization processes: comparison of characterization and mechanism of naproxen adsorption in water. Sci Total Environ 726:137828. https://doi.org/10.1016/j.scitotenv.2020.137828
31. Puga A, Moreira MM, Pazos M, Figueiredo SA, Sanromán MA, Matos CD, Rosales E (2022) Continuous adsorption studies of pharmaceuticals in multicomponent mixtures by agroforestry biochar. J Environ Chem Eng 10:106977. https://doi.org/10.1016/j.jece.2021.106977
32. Shin J, Kwak J, Lee Y-G, Kim S, Choi M, Bae S, Lee S-H, Park Y, Chon K (2021) Competitive adsorption of pharmaceuticals in lake water and wastewater effluent by pristine and NaOH-activated biochars from spent coffee wastes: contribution of hydrophobic and π-π interactions. Environ Pollut 270:116244. https://doi.org/10.1016/j.envpol.2020.116244
33. Ngo DNG, Chuang X-Y, Huang C-P, Hua L-C, Huang C (2023) Compositional characterization of nine agricultural waste biochars: The relations between alkaline metals and cation exchange capacity with ammonium adsorption capability. J Environ Chem Eng 11:110003. https://doi.org/10.1016/j.jece.2023.110003
34. Zhang J, Lu M, Wan J, Sun Y, Lan H, Deng X (2018) Effects of pH, dissolved humic acid and $Cu^{2+}$ on the adsorption of norfloxacin on montmorillonite-biochar composite derived from wheat straw. Biochem Eng J 130:104–112. https://doi.org/10.1016/j.bej.2017.11.018
35. Xu H, Han Y, Wang G, Deng P, Feng L (2022) Walnut shell biochar based sorptive remediation of estrogens polluted simulated wastewater: characterization, adsorption mechanism and degradation by persistent free radicals. Environ Technol Innov 28:102870. https://doi.org/10.1016/j.eti.2022.102870
36. Kabak B, Kendüzler E (2022) Synthesis, characterization and adsorption/sensing applications of novel cadmium (II) based coordination polymer. J Environ Chem Eng 10:107989. https://doi.org/10.1016/j.jece.2022.107989
37. Langmuir I (1918) The adsorption of gases on plane surfaces of glass, mica and platinum. J Am Chem Soc 40:1361–1403
38. Watwe V, Kulkarni S, Kulkarni P (2023) Development of dried uncharred leaves of ficus benjamina as a novel adsorbent for cationic dyes: Kinetics, isotherm, and batch optimization. Ind Crops Prod 195:116449. https://doi.org/10.1016/j.indcrop.2023.116449
39. Chowdhury S, Misra R, Kushwaha P, Das P (2011) Optimum sorption isotherm by linear and non-linear methods for safranin onto alkali-treated rice husk. Bioremediat J 15:77–89. https://doi.org/10.1080/10889868.2011.570282
40. Freundlich H (1907) Über die Adsorption in Lösungen. Z fur Phys Chem 57:385–470
41. Lagergren SK, Sven K (1898) About the theory of so-called adsorption of soluble substances. Vetensk Handl 24:1–39
42. Blanchard G, Maunaye M, Martin G (1984) Removal of heavy metals from waters by means of natural zeolites. Water Res 18:1501–1507
43. McLintock IS (1967) The elovich equation in chemisorption kinetics. Nature 216:1204
44. Debnath S, Das R (2023) Strong adsorption of CV dye by Ni ferrite nanoparticles for waste water purification: Fits well the pseudo second order kinetic and freundlich isotherm model. Ceram Int 49:16199–16215. https://doi.org/10.1016/j.ceramint.2023.01.218
45. Smiljanić D, Gennaro B, Daković A, Galzerano B, Germinario C, Izzo F, Rottinghaus GE, Langella A (2021) Removal of non-steroidal anti-inflammatory drugs from water by zeolite-rich composites: the interference of inorganic anions on the ibuprofen and naproxen adsorption. J Environ Manage 286:112168. https://doi.org/10.1016/j.jenvman.2021.112168
46. Schmidt MP, Ashworth DJ, Celis N, Ibekwe AM (2023) Optimizing date palm leaf and pistachio shell biochar properties for antibiotic adsorption by varying pyrolysis temperature. Bioresour Technol 21:101325. https://doi.org/10.1016/j.biteb.2022.101325
47. Wang H, Al-Kurdhani JMH, Ma J, Wang Y (2023) Adsorption of $Zn^{2+}$ ion by macadamia nutshell biochar modified with carboxymethyl chitosan and potassium ferrate. J Environ Chem Eng 11:110150. https://doi.org/10.1016/j.jece.2023.110150

48. Yin G, Chen X, Sarkar B, Bolan NS, Wei T, Zhou H, Wang H (2023) Co-adsorption mechanisms of Cd(II) and As(III) by an Fe-Mn binary oxide biochar in aqueous solution. J Chem Eng 466:143199. https://doi.org/10.1016/j.cej.2023.143199
49. Song X, Li K, Ninga P, Wang C, Sun X, Tang L, Ruan H, Han S (2017) Surface characterization studies of walnut-shell biochar catalysts for simultaneously removing of organic sulfur from yellow phosphorus tail gas. Appl Surf Sci 425:130–140. https://doi.org/10.1016/j.apsusc.2017.06.328
50. Zhou S, Wei Y, Li B, Wang H (2019) Cleaner recycling of iron from waste copper slag by using walnut shell char as green reductant. J Clean Prod 217:423–431. https://doi.org/10.1016/j.jclepro.2019.01.184
51. Quan C, Wang W, Su J, Gao N, Wu C, Xu G (2023) Characteristics of activated carbon derived from camellia oleifera cake for nickel ions adsorption. Biomass Bioenergy 171:106748. https://doi.org/10.1016/j.biombioe.2023.106748
52. Turk Sekulic M, Boskovic N, Slavkovic A, Garunovic J, Kolakovic S, Pap S (2019) Surface functionalised adsorbent for emerging pharmaceutical removal: adsorption performance and mechanisms. Process Saf Environ 125:50–63. https://doi.org/10.1016/j.psep.2019.03.007
53. Diao R, Zhu X, Wang C, Zhu X (2020) Synergistic effect of physicochemical properties and reaction temperature on gasification reactivity of walnut shell chars. Energy Convers Manag 204:112313. https://doi.org/10.1016/j.enconman.2019.112313
54. Boudraa I, Bougherara H, Cheurfi W, Kebabi B (2017) Characterization of the sludge of Batna (Algeria) waste water treatment plant for its valorization. J New Technol Mater 7:64–68. https://doi.org/10.12816/0044037
55. Thommes M, Kaneko K, Neimark AV, Olivier JP, Reinoso FR, Rouquerol J, Sing KSW (2015) Physisorption of gases, with special reference to the evaluation of surface area and pore size distribution (IUPAC Technical Report). Pure Appl Chem 87:1051–1069. https://doi.org/10.1515/pac-2014-1117
56. Sun S, Cao J, Xu Z, Yang Z, Xiong W, Song P, Zhong R, Peng S (2020) Porous biochar derived from waste distiller's grains for hexavalent chromium removal: adsorption performance and mechanism. J Solid State Chem 289:121492. https://doi.org/10.1016/j.jssc.2020.121492
57. Ai L, Li M, Li L (2011) Adsorption of methylene blue from aqueous solution with activated carbon/cobalt ferrite/alginate composite beads: kinetics, isotherms, and thermodynamics. J Chem Eng Data 56:3475–3483. https://doi.org/10.1021/je200536h
58. Naranjo CEA, Aldás MB, Cabrera G, Guerrero VH (2021) Caffeine removal from synthetic wastewater using magnetic fruit peel composites: material characterization, isotherm and kinetic studies. Environ Chall 5:100343. https://doi.org/10.1016/j.envc.2021.100343
59. Sips R (1948) The structure of a catalyst surface. J Chem Phys 16:490–495. https://doi.org/10.1063/1.1746922
60. Tempkin MJ, Pyzhev V (1940) Kinetics of ammonia synthesis on promoted iron catalysts. Acta Physicochim URSS 12:217–222
61. Cimirro NFGM, Lima EC, Cunha MR, Thue PS, Grimm A, Reis GS, Rabiee N, Saeb MR, Keivanimehr F, Habibzadeh S (2022) Removal of diphenols using pine biochar. Kinetics, equilibrium, thermodynamics, and mechanism of uptake. J Mol Liq 364:119979. https://doi.org/10.1016/j.molliq.2022.119979
62. Fard MA, Barkdoll B (2018) Using recyclable magnetic carbon nanotube to remove micropollutants from aqueous solutions. J Mol Liq 249:193–202. https://doi.org/10.1016/j.molliq.2017.11.039